Binding of Cross-Linked Glycosylphosphatidylinositol-Anchored Proteins to Discrete Actin-Associated Sites and Cholesterol-Dependent Domains

Kenichi Suzuki and Michael P. Sheetz
Department of Cell Biology, Duke University Medical Center, Durham, North Carolina 27710 USA

ABSTRACT The mechanism by which cross-linked glycosylphosphatidylinositol (GPI)-anchored proteins are immobilized has been a mystery because both the binding to a transmembrane protein and attachment to a rigid cytoskeleton are needed. Using laser tweezers surface scanning resistance (SSR) technology, we obtained physical evidence for cross-linked GPI-anchored protein, Qa-2, binding to a transmembrane protein and for diffusion to discrete cytoskeleton attachment sites. At low levels of cross-linking of Qa-2 molecules, the resistance to lateral movement was that expected of monomeric lipid-anchored proteins, and no specific binding to cytoskeleton-attached structures was observed. When aggregates of the GPI-anchored protein, Qa-2, were scanned across plasma membranes, the background resistance was much higher than expected for a GPI-anchored protein alone and submicron domains of even higher resistance were observed (designated as elastic or non-elastic barriers) at a density of 82 (61 elastic and 21 small non-elastic barriers) per 100 μm^2. Elastic barriers involved weak but specific bonds to the actin cytoskeleton (broken by forces of 2 or 4 pN and were removed by cytochalasin D). Small non-elastic barriers (50–100 nm) depended upon membrane cholesterol and were closely correlated with caveolae density. Thus, cross-linked GPI-anchored proteins can diffuse through the membrane in complex with a transmembrane protein and bind weakly to discrete cytoskeleton attachment sites either associated with flexible actin networks or sphingolipid-cholesterol rich microdomains in live cell membranes. Our SSR measurements provide the first description of the physical characteristics of the interactions between rafts and stable membrane structures.

INTRODUCTION

Cell plasma membranes are compartmentalized into domains where components are concentrated for signaling, transport, or other functions (Sheetz, 1993; Kusumi et al., 1999; Edidin, 1997; Jacobson and Dietrich, 1999). In recent years, sphingolipid-cholesterol microdomains, called "lipid rafts," have been identified as the platforms of a number of signaling events (Simons and Ikonen, 1997; Stauffer and Meyer, 1997; Brown, 1998). Glycosylphosphatidylinositol (GPI)-anchored proteins, which are enriched in detergent-insoluble complexes in cold Triton X-100, are postulated to be raft components, and the lipid rafts are believed to recruit components of caveolae (Simons and Ikonen, 1997). Fluorescence resonance energy transfer (FRET) microscopy has shown that the liganded folate receptor (a GPI-anchored protein) is organized in submicron domains upon overexpression in CHO cell membranes (Varma and Mayor, 1998). Evidence for the existence of rafts in vivo was also obtained by chemical cross-linking of GPI-anchored proteins (Friedrichson and Kurzchalia, 1998). High-resolution single particle tracking methodology has revealed evidence for raft-associated single molecules of GPI-anchored proteins that have restricted diffusion on BHK-21 cell membranes (Pralle et al., 2000). Another method for visualizing the microdomains was antibody cross-linking, which produced extensive protein aggregation and colocalization of many GPI-anchored proteins (Harder et al., 1998). Both ligand binding and cross-linking could cause the GPI-anchored proteins to bind to components in existing rafts (caveolae) (Lisanti et al., 1999) or to form new rafts (Harder et al., 1998; Harder and Simons, 1999) and trigger signal transduction (Hahn and Soloski, 1989; Stefanova et al., 1991; Solomon et al., 1996; Murray and Robbins, 1998). However, in all of these phenomena it is not known how the aggregation and/or liganding of GPI-anchored proteins leads to association with caveolae or to downstream signaling. In the case of integrins and cadherins, ligand binding to cross-linked transmembrane proteins results in rapid, reversible immobilization by attachment to the cytoskeleton (Kusumi et al., 1999; Felsenfeld et al., 1996; Choquet et al., 1997). This is consistent with a rapid induction event leading to cytoskeletal linkage, which is necessary because ligands for integrins and cadherins are often fixed to external matrix or cell sites. In a similar way ligand-induced cross-linking of receptors is thought to recruit downstream effectors in the signaling pathways. In the case of GPI-anchored proteins, there is a problem of how outer leaflet proteins can transduce signals to the inner leaflet. Several hypotheses, including interaction of GPI-anchored proteins with transmembrane proteins, coupling of cholesterol-rich domains between the outer and inner bilayer leaflets (Bagatolli and Gratton, 2000; Korlach et al., 1999), and interaction of alkyl chains of the outer and inner leaflets, have been proposed (Brown, 1998). Physical measurements of membrane protein movements should be performed because they can define many of the steps following aggregation that lead

Received for publication 13 March 2001 and in final form 2 July 2001.

Address reprint requests to Dr. Michael P. Sheetz, Department of Biological Sciences, Box 2408, 1212 Amsterdam Ave., Sherman Fairchild Ctr., Rm. 713, Columbia University, New York, NY 10027. Tel.: 212-854-4857; Fax: 212-865-8246; E-mail: ms2001@columbia.edu.

0006-3495/01/10/2181/09 $2.00

to signaling, caveolae binding, and lateral complex formation.

Previous studies of plasma membrane lipids on the outer leaflet have shown that they are freely diffusing with high-diffusion coefficients. GPI-anchored proteins have a wider range of diffusion coefficients and often show considerable decrease in diffusion coefficient upon cross-linking (Suzuki et al., 2000). Recent studies showed that cross-linked GPI-anchored proteins can be moved over many microns on a cell surface with surface-scanning resistance (SSR) technology (Suzuki et al., 2000). In those studies, the resistance to movement was nearly 10-fold higher than expected from tracking individual molecule movements by single particle tracking (SPT), and barriers to lateral movement were observed (Suzuki et al., 2000). One explanation is the creation of larger domains by aggregation. Sphingolipid-cholesterol lipid microdomains in artificial membranes have a high viscosity (Ferraretto et al., 1997; Ge et al., 1999) and antibody-induced aggregation of domains could produce domain fusion. Neither increased resistance nor the barriers, however, could result simply from the interaction of the beads with free-floating external microdomains because the resistance to lateral movement in membranes is only weakly dependent on the size of the domain being moved (Sattman and Delbruck, 1975; Kucik et al., 1999). It is likely that extensive clustering of GPI-anchored proteins recruits transmembrane components that bind to actin (Harder and Simons, 1999) or caveolae. Because caveolin-1 associates with the F-actin cross-linking protein, filamin (Stahlhut and van Deurs, 2000), caveolae are linked to the actin cytoskeleton as well.

In this study, to elucidate the physical interaction between raft components and cell membrane structures, we performed SSR measurements of cross-linked GPI-anchored protein, major histocompatibility complex (MHC) class I molecule Qa-2 on HEPA-OVA cell membranes. We found stationary binding sites for cross-linked Qa-2 in the cell membranes that are stable for several seconds and are cholesterol-dependent.

MATERIALS AND METHODS

Cell culture, cholesterol removal, and labeling with fluorescein-dipalmitoylphosphatidylethanolamine (Fl-DPPE)

HEPA-OVA mouse hepatoma cells expressing the Qa-2 protein were kindly provided by Dr. M. Edidin. HEPA-OVA cells were cultured in Dulbecco's modified Eagle's medium (DMEM) (Gibco Laboratories, Inc., Grand Island, NY) containing 10% fetal calf serum (Gibco) and 300 μg/ml G-418 (Sigma, St. Louis, MO). After coating the growth well with 0.01% poly-L-lysine for 15 min, cells are seeded in the well (4×10^3/well) and grown for 18–30 h before each experiment. To label HEPA-OVA cells with Fl-DPPE (Molecular Probes, Eugene, OR), cells were incubated with 1 μg/ml Fl-DPPE in serum-free DMEM for 10 min at 37°C and washed with fresh DMEM. To remove cholesterol, cells were incubated in DMEM containing lipoprotein-deficient fetal bovine serum and methyl-β-cyclodextrin (2 mM) at 37°C for 60 min. Lipoprotein was removed from serum according to Schneider et al. (1985). After washing with DMEM containing lipoprotein deficient serum, cells were used for scanning experiments.

Immunofluorescence staining of caveolae

For immunostaining experiments, cells were washed with phosphate buffered saline (PBS) three times and fixed with PBS containing 3% paraformaldehyde for 45 min at room temperature. After rinsing with PBS, cells were treated with 25 mM NH_4Cl in PBS for 10 min and 0.1% Triton X-100 for 10 min to permeabilize the cell membrane. After washing the cells four times for 10 min each, the cells were incubated with PBS containing 2% BSA and 5 μg/ml anti-caveolin antibody (Transduction Laboratories, Lexington, KY) for 45 min. After washing three times, the cells were incubated with PBS containing 2% BSA and 5 μg/ml fluorescein, anti-rabbit IgG antibody (Sigma) for 60 min. After a final washing, the cells were viewed in a Zeiss Axioscope and images were recorded with a cooled CCD camera (Photometrics).

Bead preparation

Beads coated with 10 μg/ml or 2 μg/ml monoclonal antibodies were prepared as described before (Suzuki et al., 2000). Qa-2 antibody was a gracious gift from Dr. Edidin and anti-fluorescein antibody was from Molecular Probes; 0.73-μm diameter beads were used for all studies.

Microscope and laser tweezers manipulation

The cell sample was mounted on a piezoelectric stage fixed on top of a three-plate stage of the microscope (Axiovert 100s, Carl Zeiss, Oberkochen, Germany) and was illuminated by a 100 W halogen lamp. The laser trap consisted of a beam from an 11 W TEM00 near-infrared Nd-YAG (wavelength = 1064 nm) laser (model 116F; Quantronics Lasers, Hauppauge, NY). To attach the antibody-coated bead onto the cell membrane, the bead was trapped (trap stiffness was 0.08 pN/nm), then lowered and held on the cell membrane for 4 s. The bright-field image was divided to the quadrant detector (90%) and to the camera (10%). To detect and record the position signal a 12-bit A to D computer digitizer was used. The computer was programmed to display a trace of the vertical and horizontal position of the bead detected with a quadrant detector while the data were being collected. To scan the bead across the cell surface a D to A computer board was used to send voltage signals to control the position of the piezoelectric stage via a high-voltage amplifier (Wye Creek Instruments, Fredericksburg, MD).

RESULTS

Extent of cross-linking

When beads coated with an antibody to a GPI-anchored protein, MHC class I molecule Qa-2, were scanned across the membrane surface, they encountered barriers that increased the force on the beads severalfold above background before the bead broke the bond and moved forward (Fig. 1). This was not a result of the bead being bound at the cell surface because the density of barriers was at a background level when anti-fluorescein antibody beads bound to fluorescein phosphatidylethanolamine were scanned across the membrane. Because the level of binding of both anti-Qa-2 and anti-fluorescein beads was the same, we believe that the number of molecules bound was similar. The num-

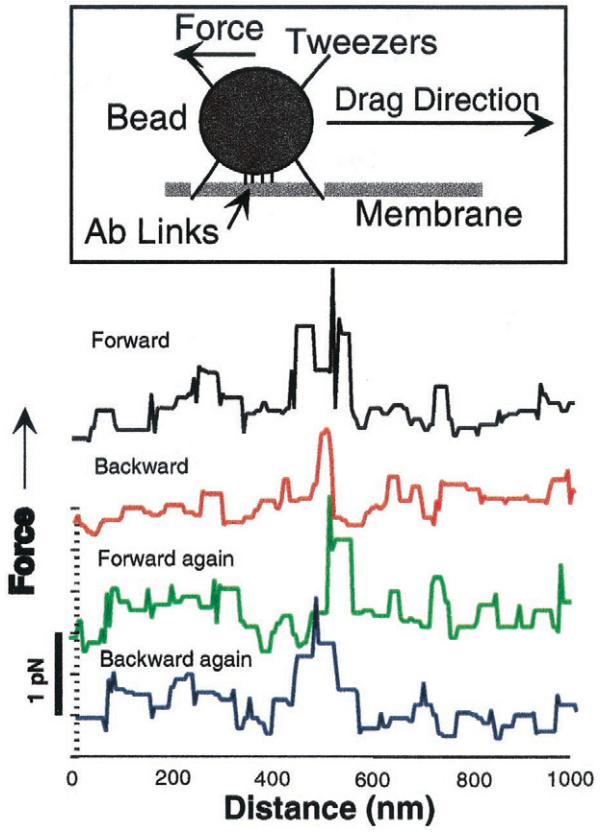

FIGURE 1 The force observed with repeated one-dimensional scans of a laser-trapped bead coated with Qa-2 antibody on HEPA-OVA cell membrane is plotted versus position. The piezoelectric stage was moved forward, backward, forward again, and backward again in one dimension at 1.0 μm/s. The position of the 0.73-μm bead attached to the membrane by the Qa-2 antibody was detected by the quadrant detector at a sampling frequency of 300 points/μm. The data were filtered using a 7-point median filter. Reproducibility of displacement was observed. In the diagram at the top, four short vertical lines coming from the bead indicate the antibody links, and four long lines coming off the bead represent optical tweezers. The direction of the bead movement is opposite to that of the drag force, as shown.

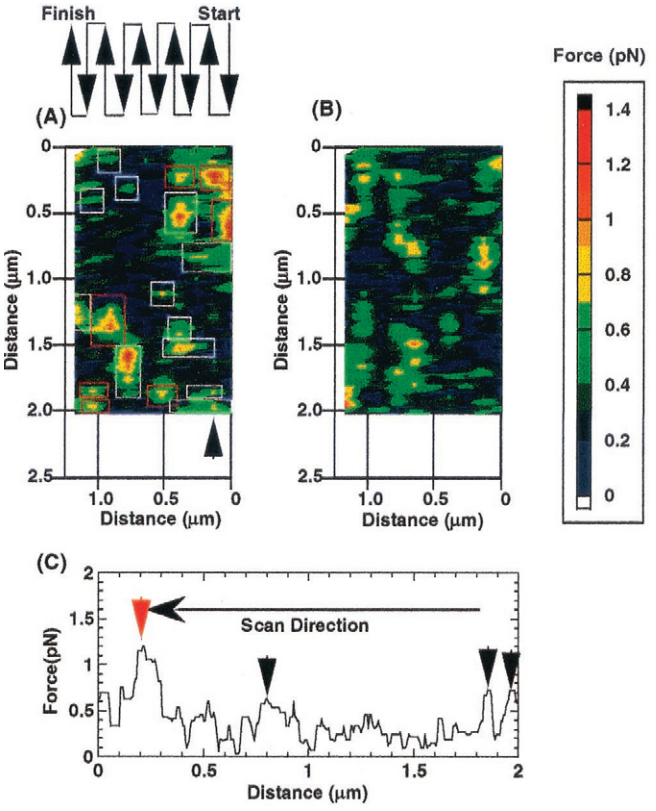

FIGURE 2 Two-dimensional scan of a laser-trapped bead coated with Qa-2 antibody on the cell membrane. Ten scans were made (five forward and five backward, with each scan separated by 130 nm laterally) using a Qa-2 antibody-coated bead at 1.0 μm/s. It took ~30 s to scan the bead across ~2 μm^2 of a membrane region (*a*), and right after the first scan was completed, the second scan (*b*) was started. Two types of barriers, non-elastic (*white square*), and elastic ones (*red square*) were observed. Even if the size of barriers was small, these were distinguishable. The bead position was detected with the quadrant detector at a sampling frequency of 300 points/μm. (*c*) Force-distance plot of the second scan lane (*arrow* in *a*). The red arrow indicates elastic barrier and black arrows mark non-elastic barriers.

ber of antibody molecules in the bead-membrane contact area (diameter = 220 nm, observed by scanning electron microscopy) was estimated to be 50 (Suzuki et al., 2000); therefore, the bead was most likely cross-linking multiple Qa-2 molecules. Assuming the linkages between the antigen and antibody followed a Poisson distribution and antibodies are randomly arrayed on the bead surface, the beads should bind at most 10 to 20 Qa-2 molecules. Thus, under the conditions used for these experiments, we suggest that the antibody beads were connected to small aggregates of Qa-2 molecules.

Definition of barriers and distribution

To characterize larger regions of cell surfaces, we examined the pattern of resistance with two-dimensional surface scans and found two distinct types of resistance features that exceeded three times the background level of resistance (the definition of barriers) (Suzuki et al., 2000). If the force increased gradually and recovered rapidly giving an asymmetric force-distance plot, the barrier was categorized as elastic (Fig. 2 *c*). If the force increased and decreased similarly with scan distance (the maximum force was close to the center of the barrier), the barrier was categorized as non-elastic (Fig. 2 *c*) (Suzuki et al., 2000). The size of the non-elastic barrier was not significantly dependent on the scanning speed, indicating that the size of non-elastic barrier is measurable by this method. The addition of cytochalasin D to alter the organization of the actin cytoskeleton decreased the density of elastic barriers to control (BSA-coated) bead levels (from 64/100 μm^2 of membrane area to 16/100 μm^2), indicating that elastic barriers are generated by the interaction between the diffusants and actin cytoskel-

etons. The larger non-elastic barriers (300–500 nm) were observed at a similar density with anti-Qa-2 and control (BSA-coated) beads (Suzuki et al., 2000), indicating that they represented nonspecific interactions and consequently were not analyzed further. The small non-elastic barriers (50–100 nm) were commonly observed with anti-Qa-2 beads (20.5/100 μm^2), but seldom with control or anti-fluorescein antibody beads on fluorescein-PE doped cells. Thus, two types of barriers (elastic and small non-elastic) are specific for cross-linked Qa-2. From earlier studies of the erythrocyte membrane, we postulated that membrane glycoproteins were corralled by cytoskeletal protein barriers (Sheetz, 1993) and it is possible that the barriers observed in our present study could form the corrals or constitute microdomains. However, the distribution of barriers was discontinuous (Fig. 2 *a*). Inelastic barriers were only 0.1–0.2 μm maximally in size, and even the larger elastic barriers were seldom seen in adjacent scans. The density of the barriers ($<1/\mu m^2$ on average) was also insufficient to significantly restrict the lateral mobility of the membrane glycoproteins over a large fraction of the cell surface.

Positioning and dynamics of barriers

If the barriers are consistently observed in the same position on the cell, they could represent specific cytoskeleton sites of interaction. When beads were scanned repeatedly over the same region at 2-s intervals (scans were made at 1 μm/s for 2 μm), there was 80% correspondence ($n = 60$) of both small non-elastic barriers (Fig. 1) and elastic barriers (not shown). Barrier stability was dependent on the actin cytoskeleton because cytochalasin D treatment significantly decreased the correspondence of non-elastic barriers to 45% ($n = 40$). Furthermore, barrier stability was very time-dependent and the barrier correspondence decreased dramatically after 30 s. Two-dimensional scans required 30 s to accumulate and we often found a dramatic change in the pattern of barriers (see Fig. 2, *a* and *b*). Correspondence of each barrier location between two successive two-dimensional scans was 9% ($n = 67$). This low correspondence could be explained by either movement of the barriers or dynamics of barriers (see Fig. 2, *a* and *b*). These results indicate that the barriers represent sites on the cytoskeleton and have a longer lifetime than a few seconds, but shorter than a minute.

The force needed to break elastic barriers is quantal

If the barriers represent specific binding sites, then we might expect to find that a quantal force is needed to break the bond. When the forces needed to break through barriers were plotted as histogram plots, peaks were observed in the plot for elastic, but not non-elastic, barriers (Fig. 3, *a–d*). At

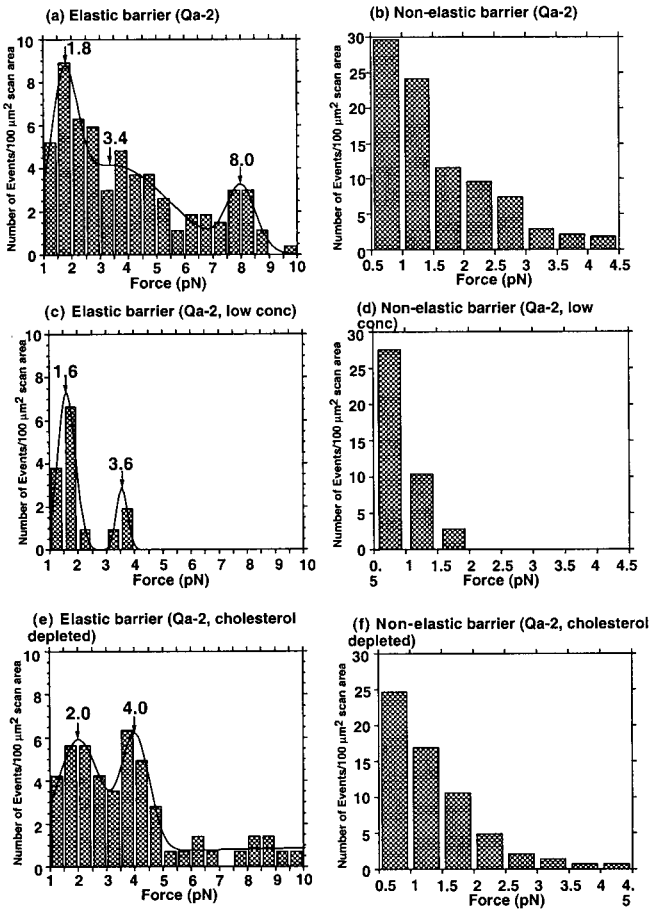

FIGURE 3 Histogram of barrier stiffness. The number of elastic barriers that released at a given force is plotted versus the force for a 0.73-μm bead coated with the normal concentration of Qa-2 antibody (10 μg/ml) either before (total scan area was 269.1 μm^2) (*a*) or after cholesterol depletion with 2 mM methyl-β-cyclodextrin for 60 min at 37°C (total scan area was 141.7 μm^2) (*e*), or coated with a low antibody concentration (2 μg/ml) (total scan area, 105.2 μm^2) (*c*). The number of non-elastic barriers that released at a given force with Qa-2 antibody (10 μg/ml) coated bead either before (*b*) or after cholesterol depletion (*f*), or with a low concentration (2 μg/ml) antibody-coated bead (*d*) were categorized by a force acting on the bead. Histograms of the elastic barrier stiffness were fit to a sum of two (*c*, *e*) or three (*a*) Gaussian distributions (*lines*). The peak, mean, and standard deviation of Gaussian functions were fit. No parameter was forced on another. The positions of the mean (*arrows*) of each Gaussian component are indicated. Multiple correlation coefficients, *R*, of the fitting are 0.973 (*a*), 0.999 (*c*), and 0.982 (*e*).

a low density of the Qa-2 antibodies on the beads (one-fifth of the normal density), peaks in the histogram were observed at 1.6 and 3.6 pN (Fig. 3 *c*), whereas at the normal antibody density, peaks were observed at 1.8, 3.4, and 8.0 pN (Fig. 3 *a*). With 10 μg/ml fluorescein antibody-coated beads attached to cross-linked Fl-DPPE molecules, elastic barriers were at the background level (6.6 barriers/100 μm^2, total scan area was 106.7 μm^2), indicating that the elastic barriers were produced by unique characteristics of the interaction between stable cytoskeletal structures and small

Qa-2 molecule aggregates. Thus, a specific bond(s) is formed that can be broken by ~2 pN/bond. Such a force is too large to be a fence effect (Sako et al., 1998; Sako and Kusumi, 1995). The spring constant of the elastic barriers, 8.4 pN/μm (median value, total number of the observed elastic barriers was 165), provides further evidence for a specific binding to the cytoskeleton. This is much larger than that of nonspecific cytoskeletal fence effects (~3 pN/μm) (Sako et al., 1998), but very similar to that observed for direct linkages between integral membrane proteins and the cytoskeleton (tether effect, ~8 pN/μm) (Sako et al., 1998). Cytochalasin D treatment did not significantly alter the spring constant of the remaining elastic barriers (median value = 9.1 pN/μm, n = 16), which is also similar to observations of the tether effect. Because the elastic spring constant was not affected by cytochalasin D and was similar between different systems, we suggest that it may represent the elasticity of a membrane-attached cytoskeletal complex. Therefore, our results are consistent with the idea that clustering of GPI-anchored proteins results in association with transmembrane proteins, which interact with a membrane-associated complex linked to the actin cytoskeleton, as previously shown in a uPAR-integrin system by biochemical methods (Xue et al., 1994). Although the nature of the transmembrane coupling protein cannot be specified in this study, the observation of discrete forces needed to break the linkages with the cytoskeleton is novel and indicates that specific bonds are formed. Furthermore, the density of the cytoskeleton binding sites is 64/100 μm^2 or on the order of 1000–2000/cell.

Small non-elastic barriers are produced by unique characteristics of cross-linked GPI-anchored Qa-2

Non-elastic barriers do not show any characteristic peaks of force in the histogram plots either at high anti-Qa-2 antibody density (Fig. 3 *b*) or low (Fig. 3 *d*). At the low antibody density on beads or with beads attached to cross-linked Fl-DPPE molecules, non-elastic barriers were scarcely observed (the number of small barriers (< 100 nm) per 100 μm^2 was 2.9 for less cross-linked Qa-2 molecules [total scan area 105.2 μm^2] and 5.8 for cross-linked Fl-DPPE molecules [total scan area 106.7 μm^2], while there were 20.5 for cross-linked Qa-2 molecules [total scan area 269.1 μm^2] and 4.6 for control [total scan area 172.1 μm^2]), indicating that the small non-elastic barriers were produced by unique characteristics of the interaction between stable membrane structures and aggregates of GPI-anchored proteins. The force needed to break through the small (<100 nm) non-elastic barriers was 2.2 ± 0.9 pN (n = 55) on average (see Discussion). The more continuous nature of the histogram plots for the small non-elastic barriers is consistent with a bonding interaction that consists of many weak interactions, which is different from the case of the elastic barriers.

The density of small non-elastic barriers is dependent on the concentration of cholesterol

Small non-elastic barriers are potentially related to sphingolipid-cholesterol-rich microdomains, including caveolae and lipid rafts. Therefore, we tested whether the density of barriers was correlated with the density of the microdomains and whether they were cholesterol-dependent. However, we cannot quantify the density of the microdomains, and instead counted the density of caveolae as an index of the density of the microdomains. Caveolae were visualized by immunostaining in the same region that was scanned by SSR. Bead scans were randomly performed over 2 μm^2 areas within the 100 μm^2 area of a cell membrane shown by the square in Fig. 4. On average, we found 20.5 non-elastic barriers per 100 μm^2 (Fig. 5 *a*, total scan area was 269.1 μm^2), whereas the number of caveolae was 32 ± 13/100 μm^2 (quantitation of distinct fluorescent punctate spots from Fig. 4 *a* and other cells [n = 18]). Upon cholesterol depletion of the cell plasma membranes with methyl-β-cyclodextrin (Harder et al., 1998), the number of the punctate spots was markedly decreased to 10 ± 4 [n = 19] (Fig. 4 *b*). The number of the small non-elastic barriers was also drastically decreased to about one-third after cholesterol depletion (Fig. 5 *b*, total scan area was 141.7 μm^2). When Fl-DPPE-bound beads were scanned (area is not shown, but the number of immunostained caveolae was similar), the small barriers were only observed at control levels (Fig. 5 *c*, total scan area was 106.7 μm^2). If the bead was not coated with antibody and not attached, but held in contact with the cell membrane, barriers were seldom observed (Fig. 5 *d*, total scan area was 172.1 μm^2) and cholesterol depletion did not alter the pattern (data not shown), which indicates that the effect of morphology on the appearance of the barrier can be neglected. These results strongly suggest that the small non-elastic barriers represent the interaction of slightly cross-linked GPI-anchored proteins with sphingolipid-cholesterol-rich microdomains. However, cholesterol depletion only reduced the elastic barriers to ~70% of normal level. The force needed to break through elastic barriers was still ~2 pN in the histogram plots (Fig. 3 *e*). Thus, cholesterol depletion caused only minor changes to the characteristics of the elastic barrier to aggregated Qa-2. Cytochalasin D treatment also reduced the number of the small (<100 nm) non-elastic barriers to 48% (9.9 small non-elastic barriers/100 μm^2) of the normal level. This result suggests that the small non-elastic barriers are linked to actin cytoskeleton.

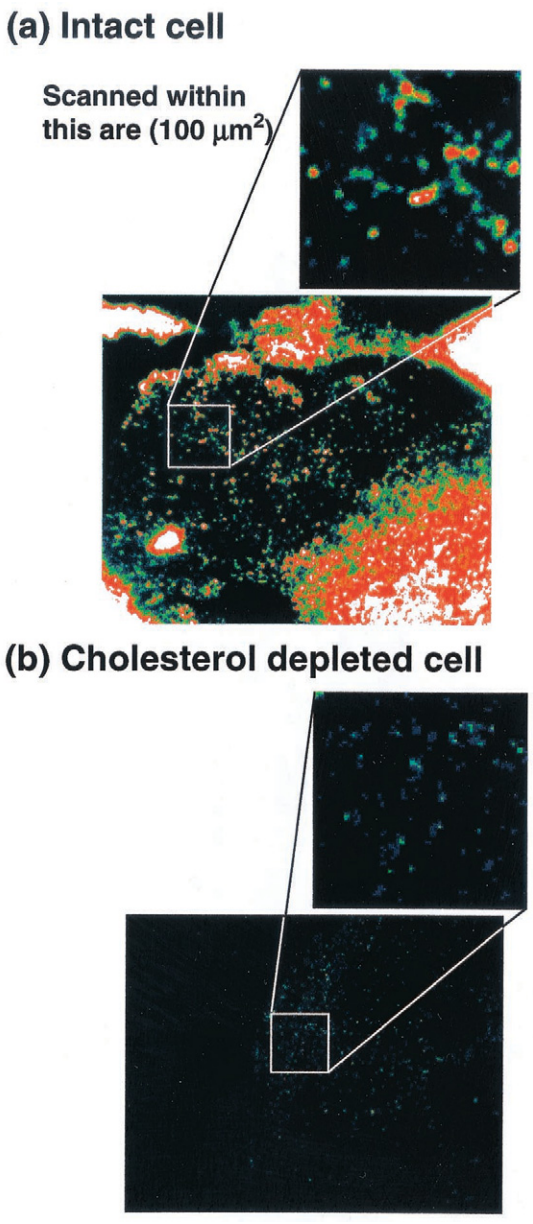

FIGURE 4 Immunofluorescence staining of caveolin. HEPA-OVA cells were fixed and immunostained for caveolin either before (*a*), or after cholesterol depletion with 2 mM methyl-β-cyclodextrin for 60 min at 37°C (*b*) as described in Methods. The number of caveolae per 100 μm^2 of membrane was determined from the number of sites with fluorescence staining intensity greater than a threshold level (see the area expanded from small white box in the main figure). In the example shown, the threshold is four contiguous green pixels. In (*a*) there are 39 areas of 0.2–0.5 μm^2 with sufficient fluorescence intensity, whereas in (*b*) there are only 11.

DISCUSSION

Two-dimensional scanning of the cross-linked GPI-anchored protein, Qa-2, provided quantification of the strength, nature, and distribution of cytoskeleton-associated binding sites. There were two types of interactions between small aggregates of Qa-2 molecules and membrane-associated cytoskeleton sites identified as elastic or non-elastic barriers (Fig. 6). In the case of elastic barriers, discrete protein-protein bonds appear to form between transmembrane proteins in the Qa-2 aggregates and sites attached to elastic actin filament networks. Displacement of the bound Qa-2 aggregates stretches the actin filament networks, resulting in a gradual rise in resistive force until the bond is disrupted and the resistive force drops to bilayer levels. In the case of non-elastic barriers, the cross-linked Qa-2 molecules bound to rigid sphingolipid-cholesterol-rich microdomains with a continuous range of interaction forces. Both types of barriers could be repeatedly measured in successive line scans of the same region separated by 2 s, but in the 30 s between successive two-dimensional scans, many of the features disappeared or moved. These findings indicate that cross-linking of GPI-anchored Qa-2 will result in binding to transmembrane proteins and the aggregates can diffuse to binding sites linked to an actin cytoskeleton network or to sites of sphingolipid-cholesterol-rich microdomains. A major advantage of the two-dimensional scans of the surface was that the structure of the barriers was defined. Not only the stiffness of the barriers, but also the two-dimensional sizes of the barriers were determined.

In all cases, the barriers to lateral movement did not define large domains or corrals, such as was postulated for erythrocyte membranes from fluorescence recovery after photobleaching (FRAP) (reviewed in Sheetz, 1993; Kusumi et al., 1999; Edidin, 1997) and SPT studies (Saxton, 1990). Discrete sites of attachment were observed for all of the barriers, with only a small fraction extending into three adjacent scan lanes. Previous studies of lateral movements of particles in one dimension (Sako and Kusumi, 1995) have observed barriers that are beneath the level of Brownian forces on 0.7 μm beads used in this study (Brownian forces are ~0.2 pN at the millisecond time scale). We could not observe cytoskeletal fences to lateral movement if they only produced very small force barriers to movement, nor would we expect to see low forces developed by lipid domains that were postulated to confine membrane protein diffusion (Bussell et al., 1995; Sheets et al., 1997; Simson et al., 1998).

The barriers that are observed by SSR of cross-linked Qa-2 molecules rather represent discrete binding sites. In the case of the elastic barriers, there are 1000–2000 sites per cell (assuming an average cell surface area of 1500–3000 μm^2). If we assume that the cross-linked Qa-2 aggregates diffuse to the sites, then they only need to diffuse 0.65 μm, which should take less than two minutes at the observed diffusion rate for the aggregates. The binding sites for the elastic barriers have a relatively low binding affinity, because the force needed to pull the aggregates off of the sites is only ~2 pN (reviewed in Carrion-Vazquez et al., 2000 and Khan and Sheetz, 1997). However, if larger aggregates of Qa-2 formed several bonds, they would dramatically increase the avidity of the binding to the cytoskeleton.

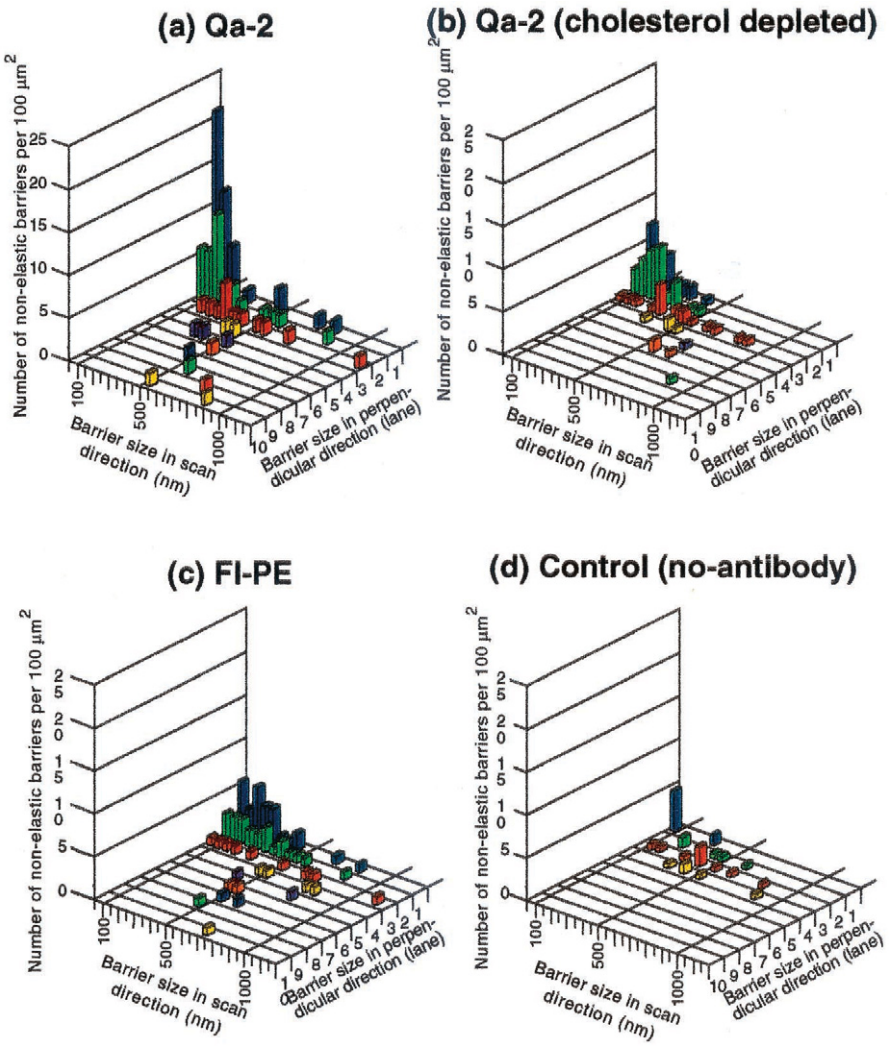

FIGURE 5 Histogram plots of non-elastic barrier sizes. Scans were performed at 1.0 μm/s with Qa-2 antibody-coated beads bound to intact HEPA-OVA cell membranes (total scan area was 269.1 μm^2) (*a*), attached to cholesterol-depleted cell membranes (total scan area was 141.7 μm^2) (*b*). Alternatively, scans were performed using an anti-fluorescein antibody-coated bead (total scan area was 106.7 μm^2) (*c*) and using a bead that is not coated with antibody, thereby not attached to the cell membrane, but contacts the membrane (total scan area was 172.1 μm^2) (*d*). The size was evaluated in terms of the scan direction and its perpendicular direction.

Because there is a dramatic shift in the force histogram plots to higher forces with higher antibody density on the beads, it is likely that larger aggregates are very strongly bound.

An actin cytoskeletal network appears to anchor the binding sites to the cell cytoskeleton, as evidenced by the elasticity of the barriers and the dependence on cytochalasin D. The much higher rigidity of the non-elastic barriers (>40 pN/μm) provides a dramatic contrast to the elastic barriers and suggests that the elastic barriers might be associated with a more dynamic portion of the cytoskeleton. Barrier reproducibility in repeated scans was decreased twofold for the elastic barriers by the depletion of cholesterol. Thus, we suggest that the elastic barriers represent binding of cross-linked Qa-2 aggregates to dynamic elements of the actin cytoskeleton that may be part of the general mechanism of clearance of cross-linked proteins from the cell surface.

Cholesterol dependence of the small non-elastic barriers indicates that they may involve sphingolipid-cholesterol-rich microdomains. Estimates of the size of microdomains range from a small number of molecules (Kenworthy et al., 2000) to 70 nm (Varma and Mayor, 1998) and the lifetimes range from subseconds to minutes (Pralle et al., 2000; Schutz et al., 2000). The density of the non-elastic barrier sites (~0.2/μm^2 in the presence and 0.06 in the absence of cholesterol) corresponds closely to that of the caveolae in the same cell regions, both in the presence and absence of cholesterol. Diffusion of an aggregate to the caveolae would take roughly threefold longer than for diffusion to the elastic barrier sites. The range of forces required to break through the non-elastic barriers is indicative of multiple weak interactions. Although it is not known if caveolae are rigidly restrained by the cytoskeleton, there are many potential

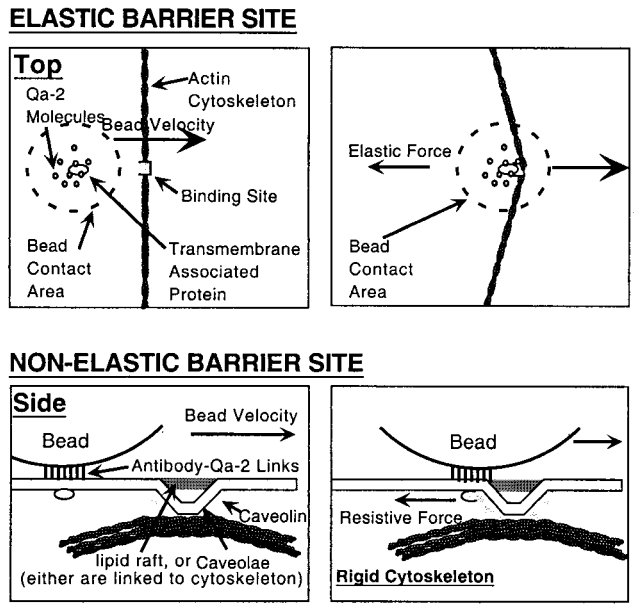

FIGURE 6 Schematic representation of two types of interaction between cross-linked Qa-2 molecules and stable (cytoskeleton-linked) membrane structures revealed by the SSR measurements. See text for details.

cytoskeleton binding proteins that could strengthen the linkage to the cytoskeleton (Stahlhut and van Deurs, 2000). Although the evidence is indirect, we suggest that the non-elastic barriers are related to the caveolae.

Two major pathways are activated in the cellular responses to GPI-anchored protein cross-linking or ligand binding: signaling and clearance. A variety of cell signal pathways are activated by cross-linking or ligand binding to GPI-anchored proteins, and many of those have been linked to caveolae (Hahn and Soloski, 1989; Stefanova et al., 1991; Solomon et al., 1996; Murray and Robbins, 1998; Parton et al., 1994). It is possible that the non-elastic barriers represent the binding of the cross-linked GPI-anchored proteins to the caveolae and the initiation of signaling. The clearance pathway is generally activated in cells when large aggregates of membrane proteins are formed. Likewise, cross-linking of GPI-anchored proteins leads to immobilization and further aggregation resulting in endocytosis (Parton et al., 1994; Verkade et al., 2000). Because the bead binding initiates the aggregation of only 15–25 Qa-2 molecules, we expect to be monitoring the early steps in the signaling or clearance pathways. It is clear that aggregation does not block diffusion nor does it seem to initiate cytoskeletal assembly on the aggregates. The change in diffusion coefficient caused by aggregation at the bead is stable for the time of the experiments. Once aggregates form, they can diffuse to binding sites that are predominantly elastic barriers in these hepatoma cells, but caveolae could predominate in other cell systems. The extent of aggregation determines the lifetime of the bond to elastic barriers, and possibly to non-elastic barriers as well. Barrier sites are very dynamic and the dynamics may be affected by binding of aggregates. Thus, at the cellular level the SSR measurements of GPI-anchored protein movements provide a clearer picture of the molecular events that could precede signaling and clearance.

In summary, SSR technology has provided the first molecular-level characterization of the binding sites of cross-linked GPI-anchored Qa-2 molecules on a live cell membrane, their size, elasticity, density, and dynamics. From the molecular details, it seems that aggregation of Qa-2 molecules recruits an additional transmembrane protein and the complex then diffuses to either elastic or non-elastic binding sites. Once bound to the different sites the cross-linked proteins could participate in signaling or cell clearance pathways.

We thank our colleague M. Edidin (Johns Hopkins University) for kindly providing us anti-Qa-2 antibody and HEPA-OVA cells. We also thank R. Sterba (Duke University) for developing the instruments and members of the Sheetz laboratory for their helpful discussions.

This work was supported by grants from the National Institutes of Health and the Muscular Dystrophy Association

REFERENCES

Bagatolli, L. A., and E. Gratton. 2000. A correlation between lipid domain shape and binary phospholipid mixture composition in free standing bilayers: a two-photon fluorescence microscopy study. *Biophys. J.* 79: 434–447.

Brown, D. 1998. Functions of lipid rafts in biological membranes. *Annu. Rev. Cell Dev. Biol.* 14:111–136.

Bussell, S. J., D. L. Koch, and D. A. Hammer. 1995. Effect of hydrodynamic interactions on the diffusion of integral membrane protein: diffusion in plasma membrane. *Biophys. J.* 68:1836–1849.

Carrion-Vazquez, M., A. F. Oberhauser, T. E. Fisher, P. E. Marszalek, H. Li, and J. M. Fernandez. 2000. Mechanical design of proteins studied by single-molecule force spectroscopy and protein engineering. *Prog. Biophys. Mol. Biol.* 74:63–91.

Choquet, D., D. Felsenfeld, and M. P. Sheetz. 1997. Extracellular matrix rigidity causes strengthening of integral-cytoskeleton linkages. *Cell.* 88:39–48.

Edidin, M. 1997. Lipid microdomains in cell surface membranes. *Curr. Opin. Struct. Biol.* 7:528–532.

Felsenfeld, D. F., D. P. Choquet, and M. P. Sheetz. 1996. Ligand binding regulates the directed movement of β1 integrins on fibroblasts. *Nature.* 383:438–440.

Ferraretto, A., M. Pitto, P. Palestini, and M. Masserini. 1997. Lipid domains in the membrane: thermotropic properties of sphingomyelin vesicles containing GM1 ganglioside and cholesterol. *Biochemistry.* 36:9232–9236.

Friedrichson, T., and T. V. Kurzchalia. 1998. Microdomain of GPI-anchored proteins in living cells revealed by crosslinking. *Nature.* 394: 802–805.

Ge, M., K. A. Field, R. Aneja, D. Holowka, B. Baird, and J. H. Freed. 1999. Electron spin resonance characterization of liquid ordered phase of detergent-resistant membranes from RBL-2H3 cells. *Biophys. J.* 77: 925–933.

Hahn, A. B., and M. J. Soloski. 1989. Anti-Qa-2-induced T cell activation. The parameters of activation, the definition of mitogenic and nonmitogenic antibodies, and the differential effects on CD4+ vs CD8+ T cell. *J. Immunol.* 143:407–413.

Harder, T., P. Scheiffele, P. Verkade, and K. Simons. 1998. Lipid domain structure of the plasma membrane revealed by patching of membrane components. *J. Cell Biol.* 141:929–942.

Harder, T., and K. Simons. 1999. Clusters of glycophosphatidylinositol-anchored proteins in lymphoid cells: accumulation of actin regulated by local tyrosine phosphorylation. *Eur. J. Immunol.* 29:556–562.

Jacobson, K., and C. Dietrich. 1999. Looking at lipid rafts? *Trends Cell Biol.* 9:87–91.

Kenworthy, A. K., N. Petranova, and M. Edidin. 2000. High-resolution FRET microscopy cholera toxin B-subunit and GPI-anchored proteins in cell plasma membranes. *Mol. Biol. Cell.* 11:1645–1655.

Khan, S., and M. P. Sheetz. 1997. Force effects on biochemical kinetics. *Annu. Rev. Biochem.* 66:785–805.

Korlach, J., P. Schwille, W. W. Webb, and G. W. Feigenson. 1999. Characterization of lipid bilayer phases by confocal microscopy and fluorescence correlation spectroscopy. *Proc. Natl. Acad. Sci. U.S.A.* 96:8461–8466.

Kucik, D. F., E. L. Elson, and M. P. Sheetz. 1999. Weak dependence of mobility of membrane protein aggregates on aggregate size supports a viscous model of retardation of diffusion. *Biophys. J.* 76:314–322.

Kusumi, A., K. Suzuki, and K. Koyasako. 1999. Mobility and cytoskeletal interactions of cell adhesion molecules. *Curr. Opin. Cell Biol.* 11: 582–590.

Lisanti, M. P., M. Sargiacomo, and P. E. Scherer. 1999. Purification of caveolae-derived membrane microdomains containing lipid-anchored signaling molecules, such as GPI-anchored proteins, H-Ras, Src-family tyrosine kinases, eNOS, and G-protein alpha-, beta-, and gamma-subunits. *Methods Mol. Biol.* 116:51–60.

Murray, E. W., and S. M. Robbins. 1998. Antibody cross-linking of the glycophosphatidylinositol-linked protein CD59 on hematopoietic cells induces signaling pathways resembling activation by complement. *J. Biol. Chem.* 273:25279–25284.

Parton, R. G., B. Joggerst, and K. Simons. 1994. Regulated internalization of caveolae. *J. Cell Biol.* 127:1199–1215.

Pralle, A., P. Keller, E.-L. Florin, K. Simons, and J. K. H. Horber. 2000. Sphingolipid-cholesterol rafts diffuse as small entities in the plasma membrane of mammalian cells. *J. Cell. Biol.* 148:997–1007.

Saffman, P. G., and M. Delbruck. 1975. Brownian motion in biological membranes. *Proc. Natl. Acad. Sci. U.S.A.* 72:3111–3113.

Sako, Y., and A. Kusumi. 1995. Barriers for lateral diffusion of transferrin receptor in the plasma membrane as characterized by receptor dragging by laser tweezers: fence versus tether. *J. Cell Biol.* 129:1559–1574.

Sako, Y., A. Nagafuchi, S. Tsukita, M. Takeichi, and A. Kusumi. 1998. Cytoplasmic regulation of the movement of E-cadherin on the free cell surface as studied by optical tweezers and single particle tracking: corralling and tethering by the membrane skeleton. *J. Cell. Biol.* 140: 1227–1240.

Saxton, M. J. 1990. Lateral diffusion in a mixture of mobile and immobile particles. A Monte Carlo study. *Biophys. J.* 58:1303–1306.

Schneider, W. J., J. L. Goldstein, and M. S. Brown. 1985. Purification of the LDL receptor. *Methods Enzymol.* 109:405–417.

Schutz, G. J., G. Kada, V. P. Pastushenko, and H. Schindler. 2000. Properties of lipid microdomains in a muscle cell membrane visualized by single molecule microscopy. *EMBO. J.* 19:892–901.

Sheets, E. D., G. M. Lee, R. Simons, and K. A. Jacobson. 1997. Transient confinement of a glycosylphosphatidylinositol-anchored protein in the plasma membrane. *Biochemistry.* 36:12449–12458.

Sheetz, M. P. 1993. Glycoprotein motility and domains in fluid plasma membranes. *Annu. Rev. Biophys. Biomol. Struct.* 22:417–431.

Simons, K., and E. Ikonen. 1997. Functional rafts in cell membranes. *Nature.* 387:569–572.

Simson, R., B. Yang, S. E. Moore, P. Doherty, F. S. Walsh, and K. A. Jacobson. 1998. Structural mosaicism on the submicron scale in the plasma membrane. *Biophys. J.* 74:297–308.

Solomon, K. R., C. E. Rudd, and R. W. Finberg. 1996. The association between glycophosphatidylinositol-anchored proteins and heterotrimeric G protein alpha subunits in lymphocytes. *Proc. Natl. Acad. Sci. U.S.A.* 93:6053–6058.

Stahlhut, M., and B. van Deurs. 2000. Identification of filamin as a novel ligand for caveolin-1: evidence for the organization of caveolin-1-associated membrane domains by the actin cytoskeleton. *Mol. Biol. Cell.* 11:325–337.

Stauffer, T. P., and T. Meyer. 1997. Compartmentalized IgE receptor-mediated signal transduction in living cells. *J. Cell. Biol.* 139: 1447–1454.

Stefanova, I., V. Horejsi, I. J. Ansotegui, W. Knapp, and H. Stockinger. 1991. GPI-anchored cell-surface molecules complexed to protein tyrosine kinases. *Science.* 254:1016–1019.

Suzuki, K., R. E. Sterba, and M. P. Sheetz. 2000. Outer membrane monolayer domains from 2-D surface scanning resistance (SSR) measurements. *Biophys. J.* 79:448–459.

Varma, R., and S. Mayor. 1998. GPI-anchored proteins are organized in submicron domains at the cell surface. *Nature.* 394:798–801.

Verkade, P., T. Harder, F. Lafont, and K. Simons. 2000. Induction of caveolae in the apical plasma membrane of Madin-Darby canine kidney cells. *J. Cell Biol.* 148:727–739.

Xue, W., A. L. Kindzelskii, R. F. Todd III, and H. R. Petty. 1994. Physical association of complement receptor type 3 and urokinase-type plasminogen activator receptor in neutrophil membranes. *J. Immunol.* 152: 4630–4640.